Science Advances
AAAS

Supplementary Materials for

Cytostatic hypothermia and its impact on glioblastoma and survival

Syed Faaiz Enam *et al.*

Corresponding author: Syed Faaiz Enam, faaiz.enam@gmail.com; Ravi V. Bellamkonda, ravi@duke.edu

Sci. Adv. **8**, eabq4882 (2022)
DOI: 10.1126/sciadv.abq4882

The PDF file includes:

Other Supplementary Material for this manuscript includes the following:

Supplementary Materials and Methods

a. Device fabrication

Device design and manufacturing was done in collaboration with the Pratt Bio-Medical Machine Shop at Duke University. Designs were developed on MasterCam and Fusion360 (fig. S6). Most materials and parts were obtained through McMaster, or vendors such as Digi-Key, Newark Element, Mouser, or Amazon.

Metal and polycarbonate parts: MasterCam designs were programmed into tool paths for a three axis CNC milling machine. Raw polycarbonate (McMaster), copper (145 copper, McMaster), and aluminum (McMaster) were used to fabricate various parts including the Interface, copper contacts, and the heat sink and its cover (fig. S6F). The tools used were .125", .0625" and 1 mm high speed steel end mills and high-speed steel drills.

Interface: This consisted of a polycarbonate base, a gold needle threaded through a copper part, and a thermistor with its ends wrapped around protected brass screws (fig. S6, H and I). The gold needle was fashioned from 24k 1-mm diameter gold wire (Hauser & Miller) with one end sharpened to a 45° angle by hand with a fine jewelers file in a small lathe using a 1-mm 5C collet. The gold was inserted through a hole in the adjoining copper part, ensuring the proper length for tumor penetration (3 mm from bottom surface of polycarbonate base). The gold was carefully soldered to the copper with minimal 40/60 standard solder into the top side. Care was taken to prevent (and remove) any excess solder wicking past the gold to ensure proper seating into the base recess. Remaining gold and solder on top were filed flush to the copper.
Next, two brass screws were inserted into the polycarbonate base and fixed with epoxy (Henkel Loctite, Ellsworth Adhesives). Then, under a dissection microscope, thermistors (Amphenol Advanced Sensors) that were either MRI-compatible (A96N4-GC11KA143L/37C) or MRI-incompatible (AB6N2-GC14KA143E/37C), were measured, cut, and stripped with a blade. The thermistors were threaded through a hole in the polycarbonate base on one end, and the wires were wrapped around the brass screws. Heat shrink was added around the wired screws, and then protected with a polycarbonate part and secured with additional epoxy. Prior to implantation, these were sterilized under UV light for 30 minutes and left in 70% ethanol overnight.

Cooler: The Cooler (fig. S6, A to E) consisted of a fan (MF20080V1-1000U-A99, Sunon), the fabricated heat sink with cover, a female connector (SM06B-GHS-TB, JST Sales America) protected by a 3D printed component (fig. S6G), a potted Peltier plate (TE-65-0.6-1.2, TeTech), and a fabricated polycarbonate plate with a copper part and steel shims (fig. S6J). The Peltier plate had thermal paste (Kryonaut, Thermal Grizzly) applied on both surfaces. For rats receiving normothermia, the Peltier plate was replaced by a block of PDMS of equivalent dimensions. An aluminum grill (9305T92, McMaster) was added above the fan to protect it from bedding. The Cooler was held together with screws.

Wiring: 26G wire was wrapped around screws that fastened the shims to the polycarbonate plate. These wires, along with the Peltier plate wires were passed through holes in the aluminum heatsink. The wires, including from the fan, were soldered to the female connector. The connector was protected with a 3D-printed part and then secured with epoxy and hot glue.

The device enabled the Cooler to be attached to the Interface such that the copper parts made contact to transfer heat, and the steel shims contacted the brass screws to complete the thermistor circuit (fig. S6, K and L).

b. Animals

All animal procedures were approved by the Duke IACUC. Fischer (CDF) and Nude (RNU) rats were purchased from Charles River at 7–9 weeks of age. All procedures began at 8–10 weeks of age.

Tumor inoculation: Tumor cells were grown *in vitro* for two passages, harvested the morning of the surgery, and kept on ice until injection. Animals were induced with 5% isoflurane anesthesia and maintained between 1–3% with visual monitoring of breathing. Buprenorphine-SR was administered subcutaneously at 1 mg/kg for pain control. Fur on the scalp was trimmed with an electric trimmer followed by removal with hair-removal cream. The head was then secured in a stereotaxic apparatus. Eye ointment was applied on the eyes. The scalp was sterilized with three alternating washes of 70% ethanol and chlorhexidine. Bupivicaine (0.25% w/v) was injected into the scalp. A central incision was made on the scalp and the skin retracted. A 0.6 mm conical burr was used to drill at -0.5 AP and + 3 ML to a depth of 0.8–0.9 mm. A Hamilton syringe with 26G needle loaded with at least 5 µL of either F98 cells (in Fischer rats) or U-87 MG cells (in RNU rats) was centered to the drill site. Prior to insertion, the tip was wiped of any hanging droplet. The needle was penetrated to a depth of 1.75 mm from the outer table of the skull and then retracted by 0.25 mm for a final location of 1.5 mm DV. Infusion was begun with a pump at 0.5 µL/min for 10 min. Upon 1 minute after completion, the syringe was slowly retracted, and the scalp sutured. The rat was then placed in the custom cage to begin accommodating. Supplemental nutritionally complete diet gel (76A, ClearH2O) was provided regularly.

Implantation: One week after inoculation, MR images were acquired was taken to confirm tumor-take. The subsequent day, the rats were prepared for implantation (fig. S8B). As previously, the rats were induced under anesthesia and buprenorphine-SR was administered subcutaneously at 1 mg/kg. The scalp was sterilized, bupivacaine (0.25% w/v) was administered, and the scalp was incised. This time, extra effort was put into retraction, scraping off the peritoneum, slightly separating the temporalis muscles, and ensuring hemostasis with etching gel (Henry Schein) and 0.4% hydrogen peroxide. Once the cranium was absent of blood and dry, burr holes were made using conical drill bits (Roboz Surgical Instruments Co.) for the gold probe, thermistor, and titanium screws (0035962, Allied Titanium). This included one burr hole with a 0.8 mm tip for the thermistor, 1.5 mm caudal from the tumor inoculation. Following this, a 1.0 mm conical burr was used 6 mm laterally from the thermistor for titanium screw (TS) 1, 4 mm caudally from TS1 for TS2, 10 mm caudally from thermistor for TS3, and 6 mm rostrally from the tumor inoculation for TS4. The original tumor inoculation burr hole was expanded to 1.4 mm. Titanium screws (filed down to be 1-mm in length) were then twisted into their holes at a depth of 0.6 mm. Next, after cleaning the skull again, the sterile Interface was gently inserted and held down while UV-curable dental cement (Henry Schein) was added to the sides and cured. Following this, layers of dental cement were added around and above the screws, Interface, and skull to secure the Interface to the skull. Upon completion, stitches were used to gently approximate the skin (including around the arms of the Interface) while keeping the surface of the Interface exposed. The rat was monitored while waking up and for 2 hours after to ensure recovery.

Attachment: Two days after recovery, the rat was put under anesthesia to attach the Cooler. A miniscule drop of thermal paste was added between the copper contacts and the Cooler was then screwed to the Interface. A patch cable was then connected to both the Cooler and the slipring hovering above the cage on a lever arm. For studies where MRI was possible, an

additional MR image was acquired at 5–7 days after implantation (with the Cooler screwed off). After this, devices were switched on; rats with a cooling device had their fan and Peltier powered ("Device ON") while rats with normothermia only had a fan that was powered ("Device OFF"). Temperature was monitored through the Arduino connected to a computer and recorded using PuTTY v0.74 (www.putty.org).

Monitoring and maintenance: The intracerebral temperatures were intermittently monitored throughout the day by connecting the computer through a local network. This enabled us to respond quickly to any sudden changes in temperature, usually due to some transient failure of the patch cable, alligator clips, or device which was rectified. Over time, there was regularly an accumulation of fur inside the heat sinks and fans. This was intermittently removed with tweezers as possible. For more complicated adjustments and corrections, the rat was put under anesthesia. Rats were given nutritionally complete diet gel regularly but were also able to eat regular food and drink water from the water bottle. Supplemental treats such as softies were also provided (Bio-Serv). Cages were cleaned once weekly. Rats were typically weighed every 2–4 days but were weighed daily if weight started falling. The procedure involved transiently disconnecting the patch cable from the slipring, moving the rat to an empty cage, and subtracting the weight of the cage, patch cable, and device.

Euthanasia: Euthanasia criteria included: 10–15% weight loss from initial weight (after recovery from Interface implantation), or signs of significant distress, porphyrin staining around the eyes, and lack of grooming and appetite. For survival studies, rats were censored if the Interface detached from the skull. When a rat reached these criteria, they were induced under 5% anesthesia and prepared for euthanasia. The patch cable and Cooler were detached. A thoracotomy was performed followed by a trans-cardial perfusion with PBS (250 mL) and then 10% formalin (250 mL). The animals were decapitated, and the skull with the brain and Interface still in place was carefully collected and left for 24 hours in 10% formalin at 4°C. Next, the Interface and skull were carefully removed, and the brain was transferred to 20% sucrose and stored at 4°C until it sunk. Subsequently, the brain was grossly sectioned, placed on an aluminum mold and buried with Optimal Cutting Temperature compound. The aluminum portion was then exposed to liquid nitrogen to initiate snap-freezing, followed by completion on dry ice. The block was stored at -80°C until further processing.

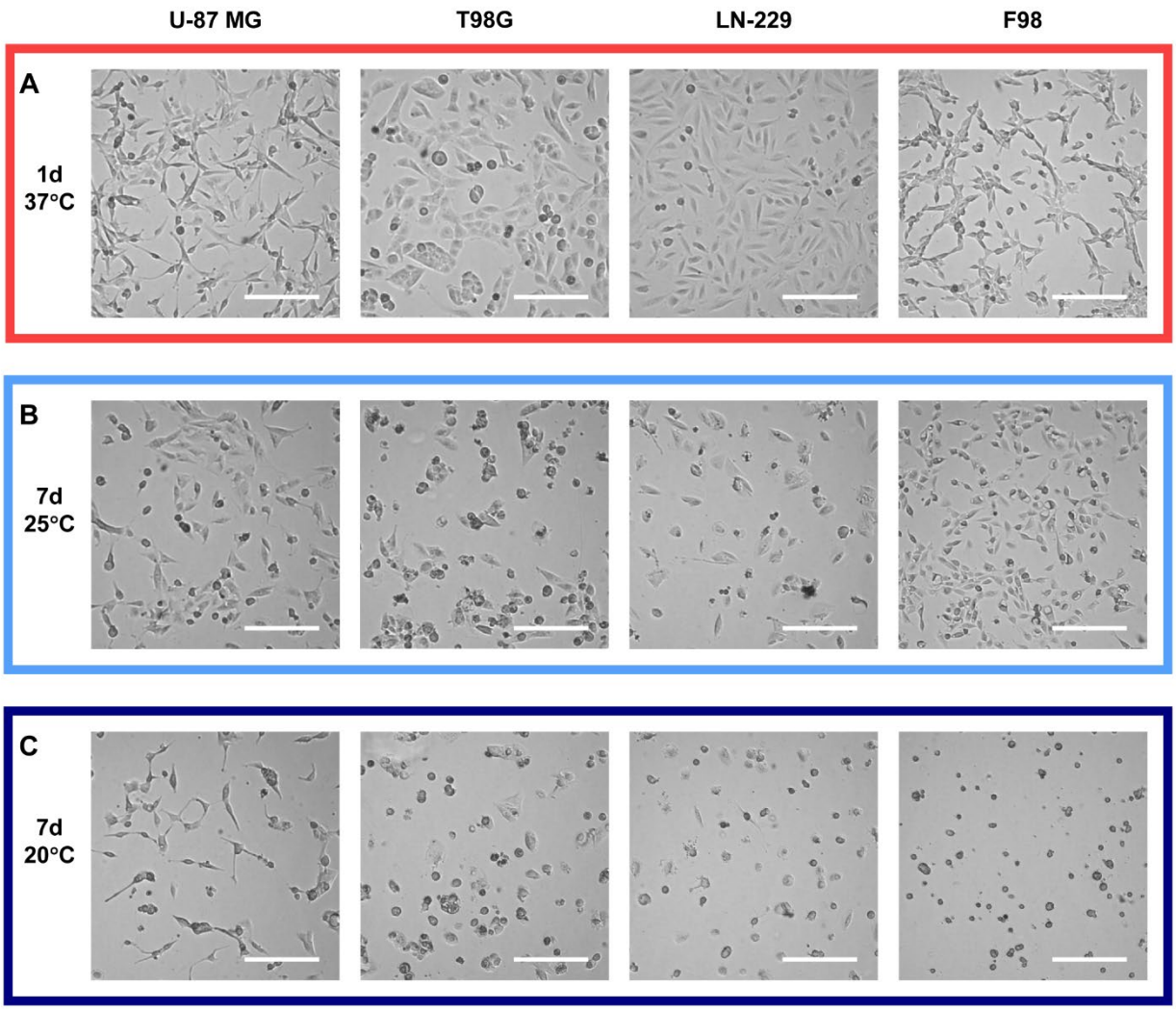

Supplementary Figure 1: Brightfield images of GBM lines under different temperature conditions. All cells received overnight incubation at 37°C and then were either left at 37°C or transferred to 25°C or 20°C. White scale bars = 250 µm. **(A)** Images of cells after 1 day at 37°C. **(B)** Images of cells after 7 days at 25°C. **(C)** Images of cells after 7 days at 20°C.

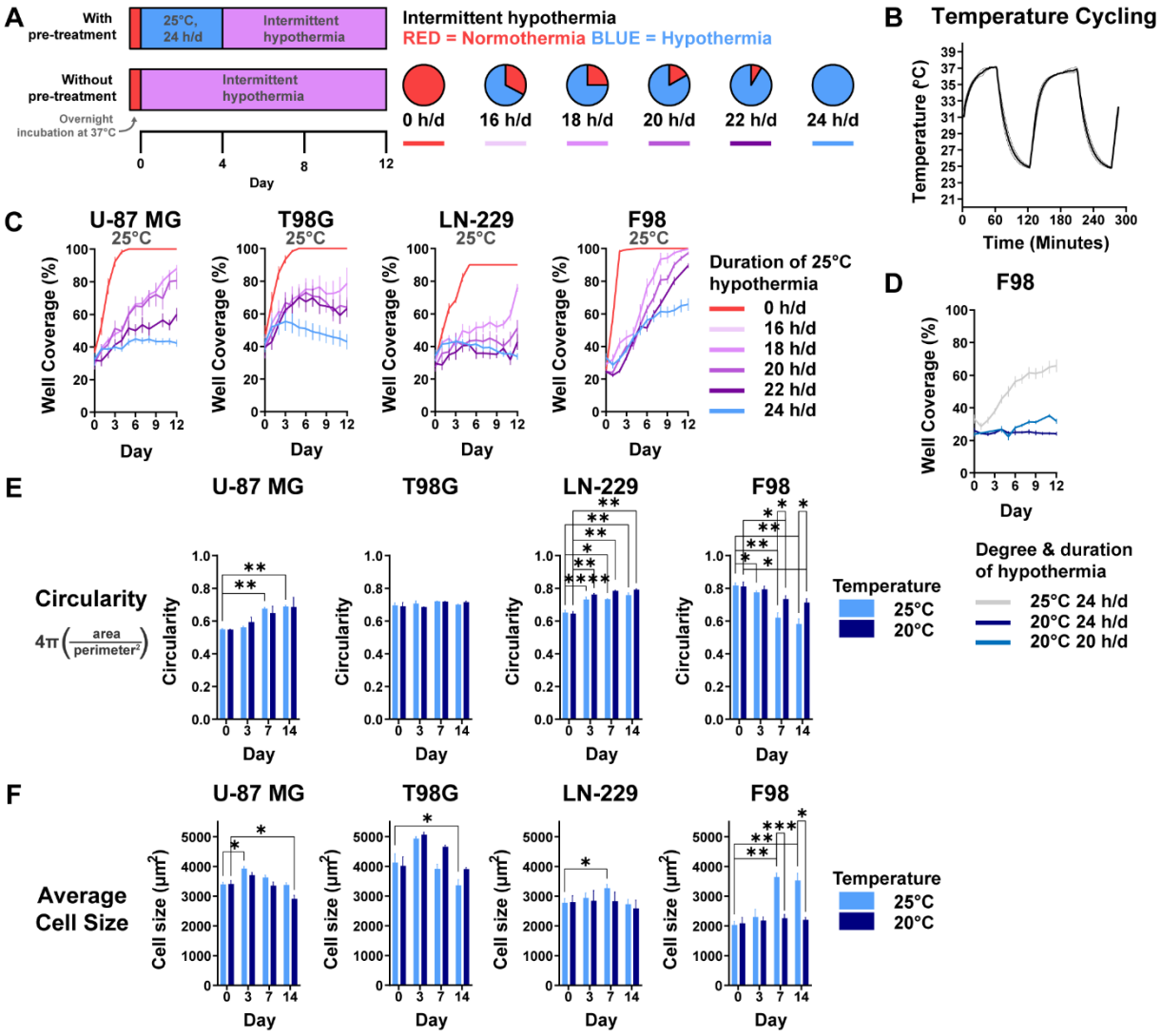

Supplementary Figure 2: Effect of intermittent hypothermia on cell growth and continuous hypothermia on cell morphology. (A) Timeline schematic of intermittent hypothermia. **(B)** Plot demonstrating the change of media temperature when a microplate is transferred between 37°C and 25°C cell incubators (n = 2). Thermistors were attached to the bottom of a central well and lateral well. Resistance was measured with a voltage-divider circuit and Arduino and converted to temperature with a script. **(C)** GBM growth rates under intermittent 25°C hypothermia without 25°C pre-treatment (n = 8 wells). Plates were transferred between 37°C and 25°C incubators for varying hours/day (h/d). **(D)** F98 growth rate under continuous 25°C or 20°C hypothermia or 20 h/d intermittent 20°C hypothermia with 4 days of 20°C pre-treatment. **(E) and (F)** Average tumor cell circularity and average size under hypothermia (n = 8 wells). Circularity and average size were determined through an ImageJ script analyzing all imaged cells in a well. Two-way ANOVAs were conducted with Dunnet's multiple comparison tests post-hoc (*p<0.05, **p<0.01, ***p<0.001, ****p<0.0001). Specific adjusted p-values are provided in Supplementary Tables 2 and 3. All graphs show mean ± standard deviation.

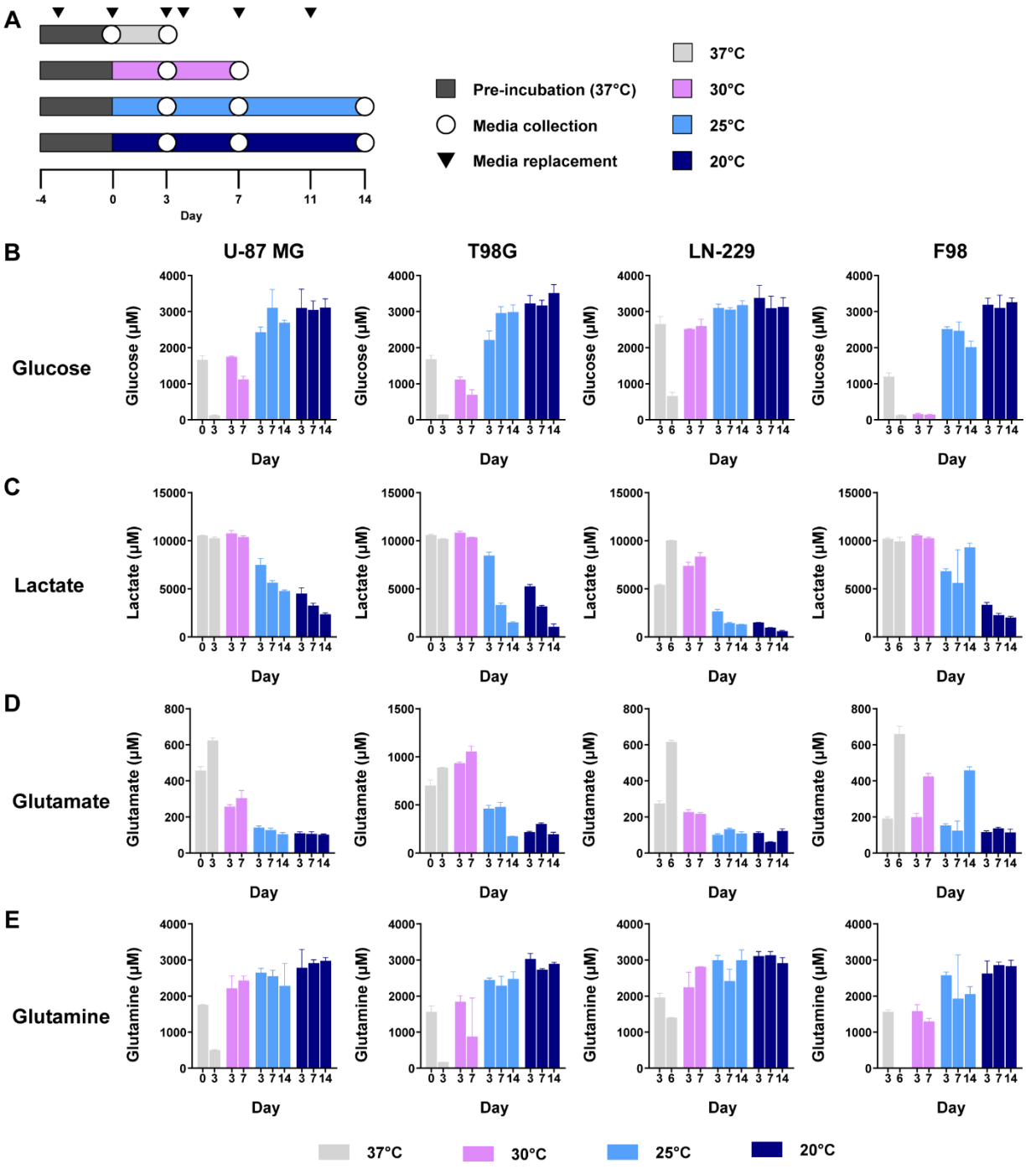

Supplementary Figure 3: Metabolite production and consumption under hypothermia. (A) Timeline schematic of metabolite assay demonstrating media replacement 3 days prior to media collection and when plates were transferred to hypothermic conditions. **(B)** Glucose levels in media at 3, 7, and 14 days at different temperatures. **(C)** Lactate levels in media at 3, 7, and 14 days at different temperatures. **(D)** Glutamate levels in media at 3, 7, and 14 days at different temperatures. **(E)** Glutamine levels in media at 3, 7, and 14 days at different temperatures. All graphs show mean ± standard deviation. Statistical analyses are provided in Supplementary Table 5.

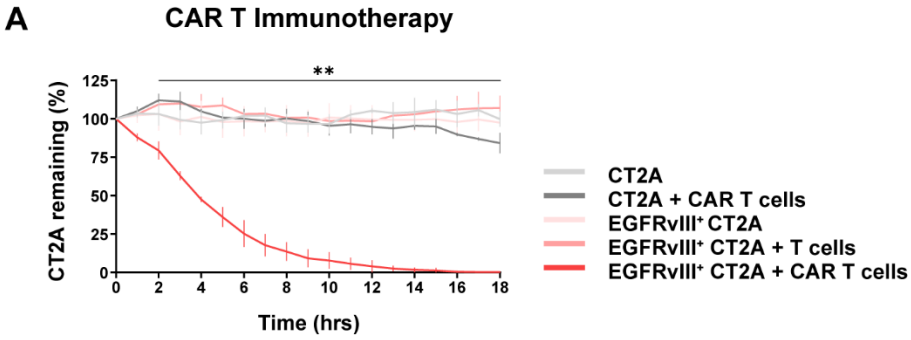

Supplementary Figure 4: Validation of CAR T cells. (A) Graph demonstrating the specific killing of EGFRvIII$^+$ CT2A cells by CAR T cells only (n = 4). Repeated measures ANOVA was conducted with Dunnett's multiple comparisons test comparing the group of EGFRvIII$^+$ CT2A cells with CAR T cells to EGFRvIII$^-$ CT2A only (**$p < 0.01$ at least in all comparisons).

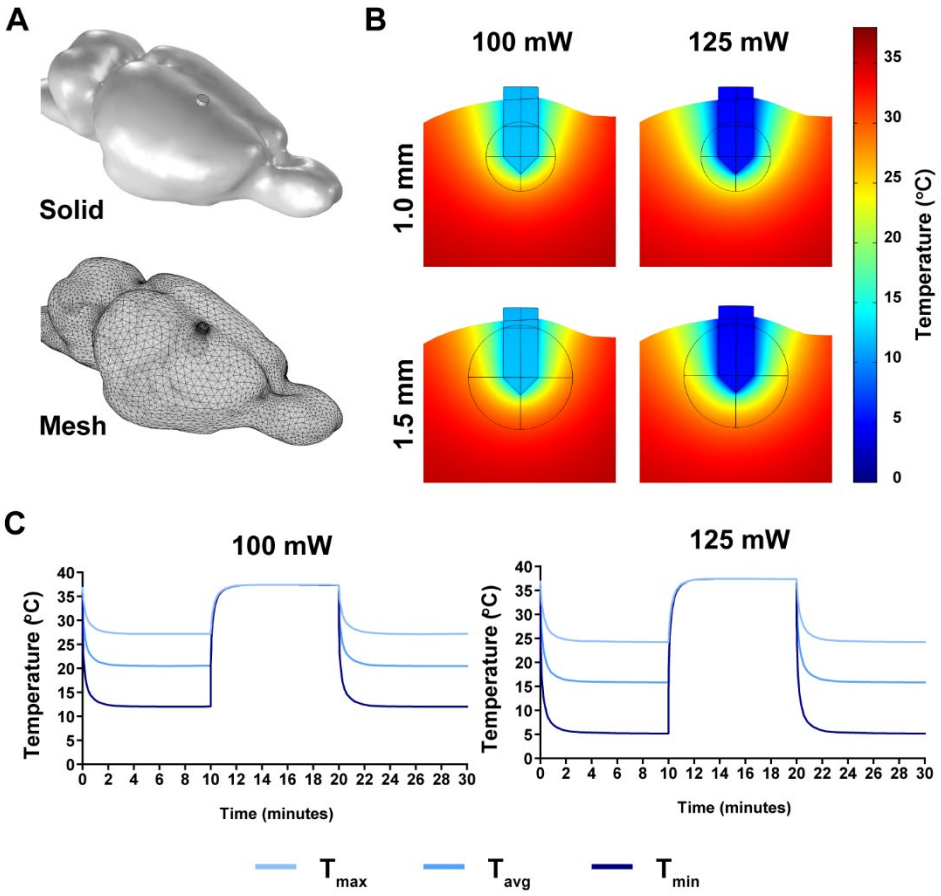

Supplementary Figure 5: Finite-element analysis of local intratumoral hypothermia. (A) Above: Smoothened rat brain model obtained from the literature with the addition of a probe and tumor. Below: fine mesh added to the model for finite-element analysis. **(B)** Coronal slices depicting degree and extent of hypothermia depending on tumor size (1 mm and 1.5 mm radius) and heat energy pulled (100 and 125 mW). **(C)** Time-dependent study modeling maximum, average, and minimum tumor temperatures over time. Cooling was begun at t = 0, stopped at t = 10, and restarted at t = 20 minutes.

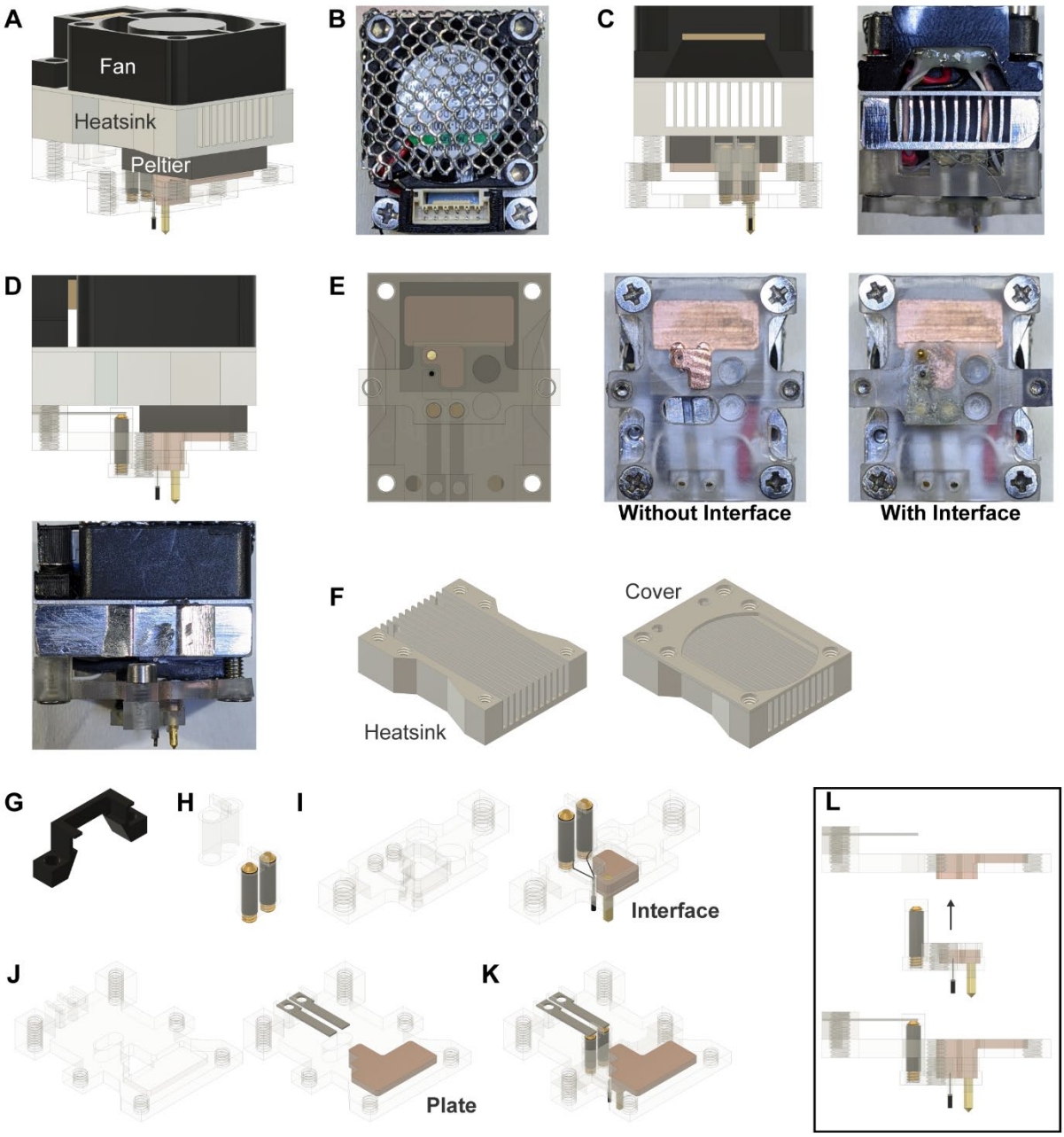

Supplementary Figure 6: Local hypothermia rodent device. (A) Rendered front angle view of device. **(B)** Top view of device. Aluminum mesh is visible above a fan. Beige connector is visible surrounded by a 3D printed cover. **(C)** Rear view of device. Left: render. Right: picture shows wires terminating at connector where they were soldered and protected with epoxy. **(D)** Side view of device. All components are visible with this perspective. **(E)** Bottom view of device. Left: render. Middle: Picture including the presence of Interface. Right: Picture without the Interface. Steel shims, Peltier wires, and copper part are visible through the polycarbonate base. **(F)** Render of heat sink without cover (above) and with cover (below). Holes were drilled to enable passage of wires and fastening of screws. **(G)** Render of 3D-printed component to secure the beige connector. **(H)** Render of polycarbonate part to protect the heat-shrink covered brass screws. **(I)** Render of polycarbonate Interface base alone (left) and with all parts (right). Thermistor wires are wrapped around the brass screws under the heat shrink. Copper part with gold needle is pressed into the polycarbonate base. **(J)** Render of polycarbonate plate of Cooler alone (left) and with all parts (right). Steel shims are components of the thermistor circuit. **(K) and (L)** Renders of Interface and polycarbonate plate of Cooler as they are contacted together to enable heat conduction and closing the thermistor circuit.

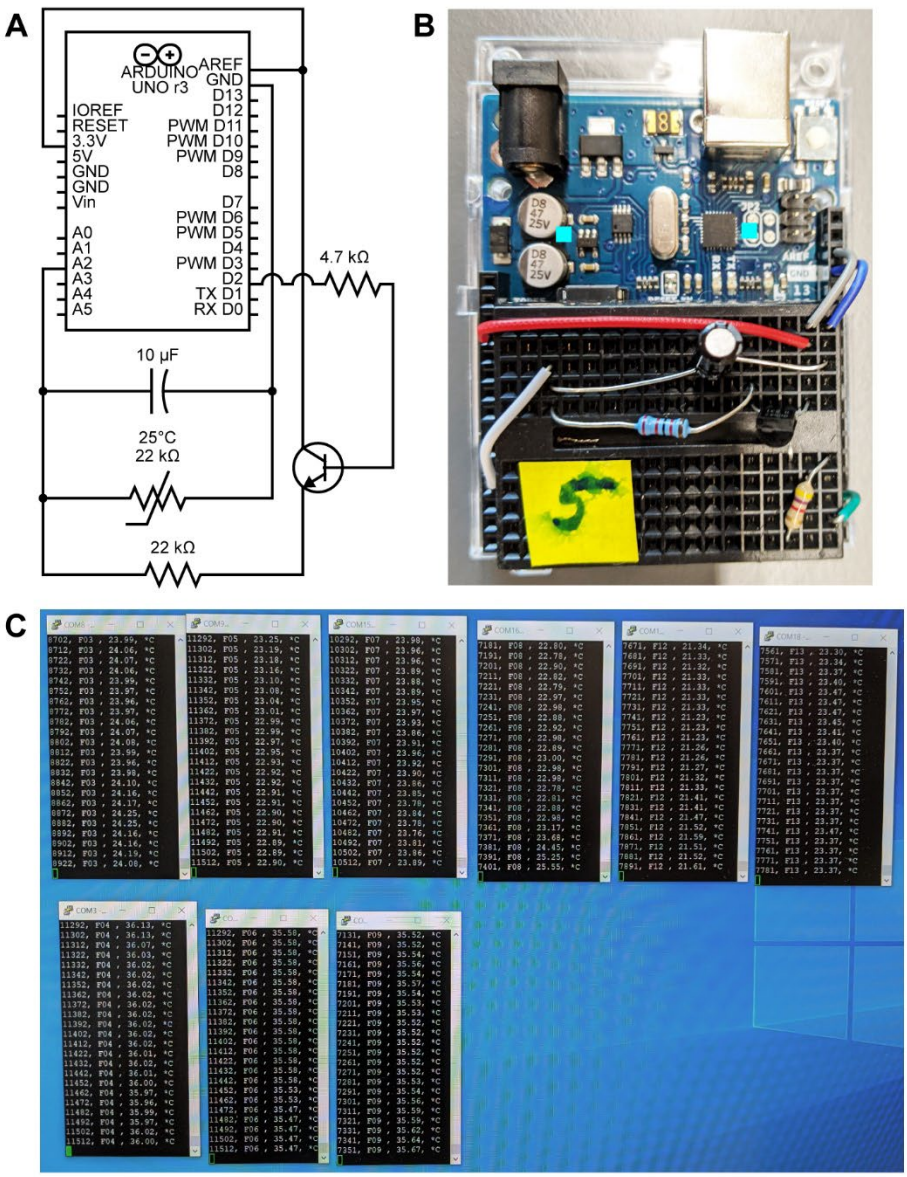

Supplementary Figure 7: Thermistor circuit for temperature monitoring. (A) Schematic demonstrating the voltage-divider circuit used to measure resistance across the thermistor. A digital pin from the Arduino was used to take intermittent and averaged recordings (every 10s). **(B)** Photo of voltage-divider circuit on a breadboard above the Arduino. One of these was used per rat for temperature monitoring. Arduino code converted the resistance across the thermistor to temperature using a manufacturer supplied beta-value. **(C)** Picture of computer screen depicting continuous temperature monitoring through PuTTY. The computer was also connected to the network to enable temperature monitoring outside the vivarium.

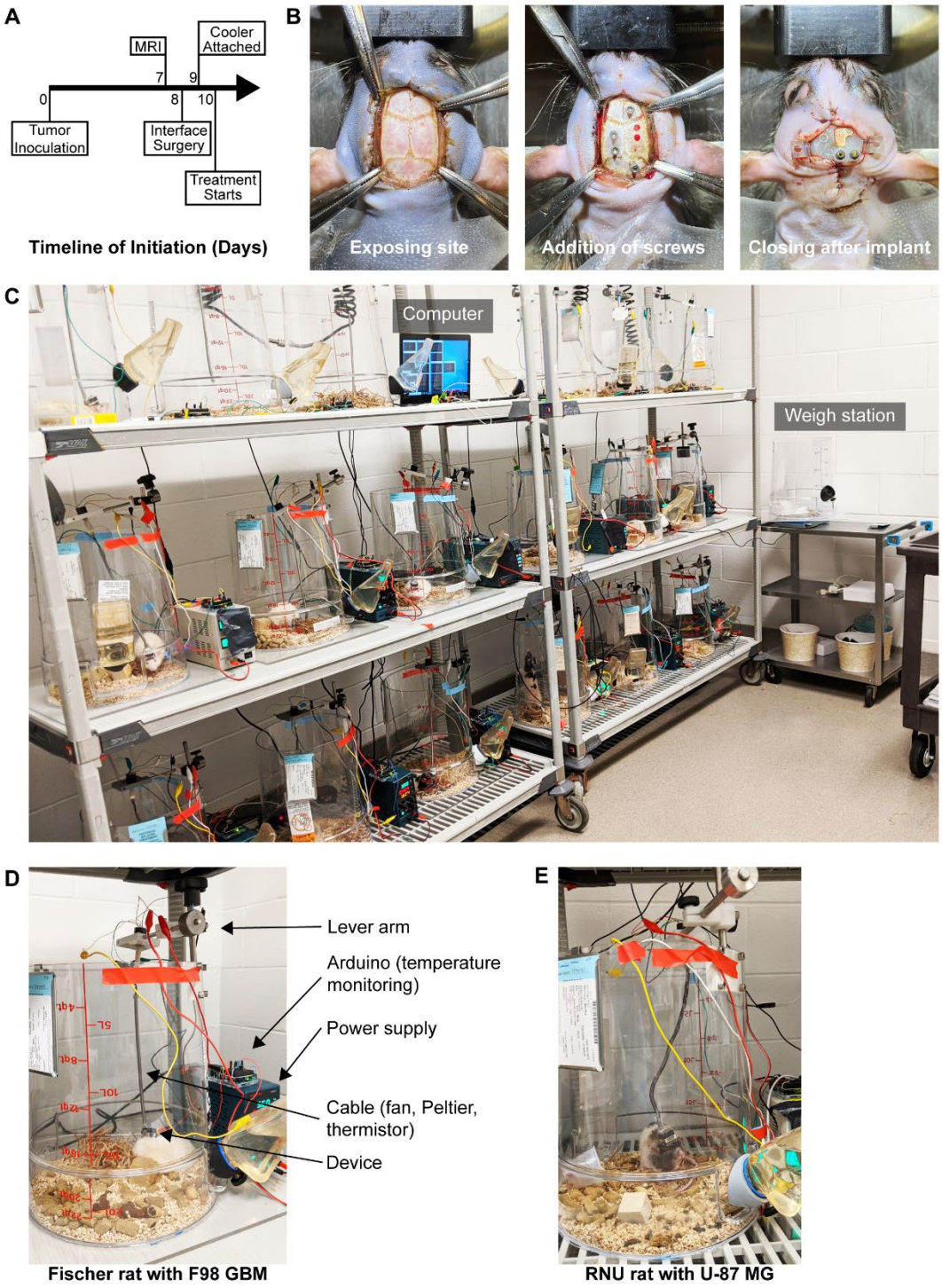

Supplementary Figure 8: *In vivo* Interface implantation and treatment application. (A) Timeline of tumor inoculation, MRI, Interface implant surgery, Cooler attachment, and treatment initiation. **(B)** Photos of implantation surgery in an RNU rat 8 days after tumor inoculation. Left: the surgical site is re-exposed and hemostasis established. Middle: burr holes were drilled for the intratumoral probe, thermistor, and four titanium screws. The titanium screws were tightened by hand. Right: suturing around the Interface which was attached to the skull using dental cement. The copper part for heat conduction and the brass screws are visible for contact with the Cooler. **(C)** Set up of multiple cages, power supplies, temperature monitoring, and a central computer in the vivarium. Rats were weighed in an empty cage visible on the right. **(D)** Photo of a Fischer rat under treatment. Patch cable, slip ring, lever arm, power supply, and water bottle are visible. **(E)** Nude (RNU) rat under treatment.

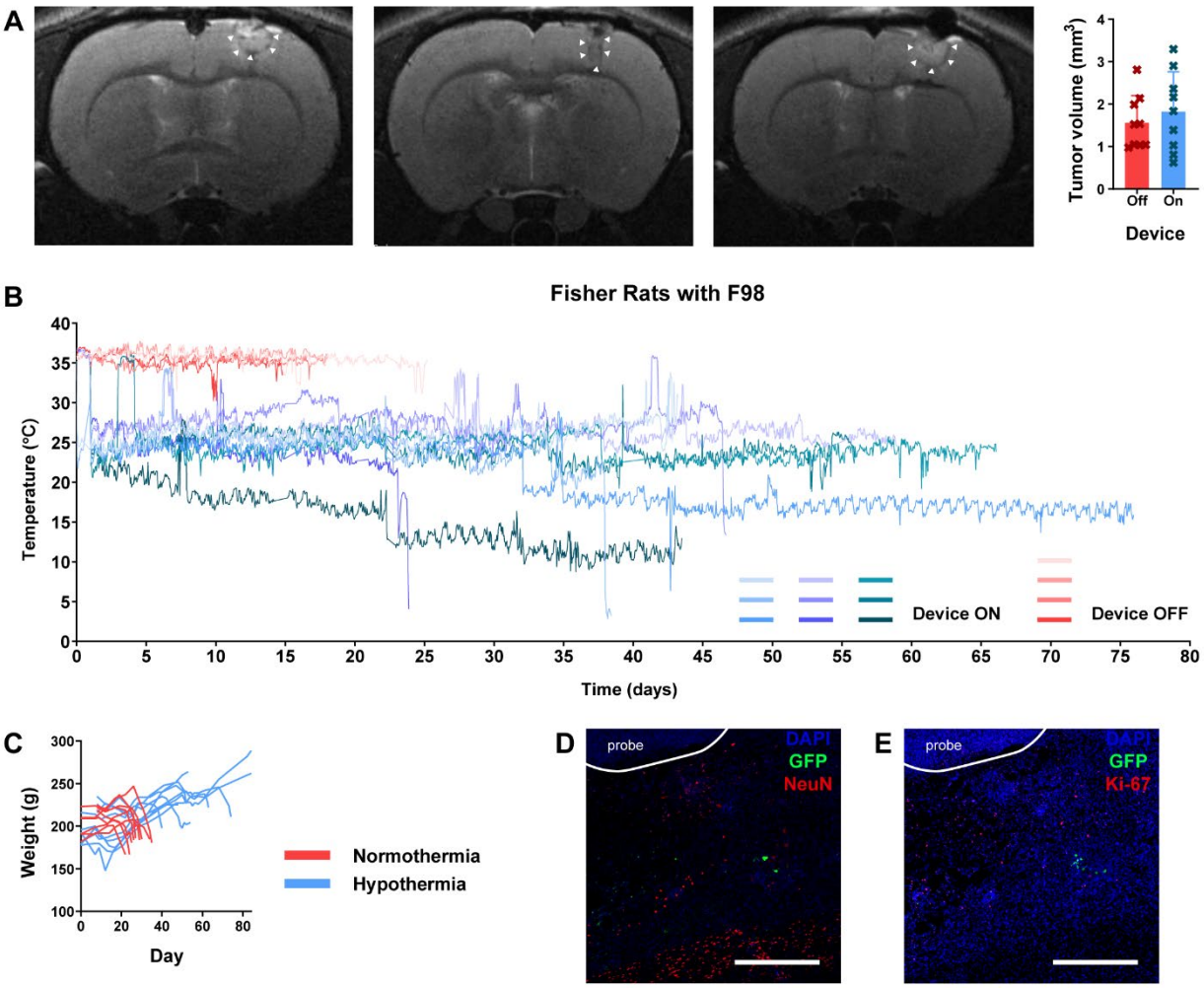

Supplementary Figure 9: Hypothermia treatment of Fischer rats inoculated with F98 GBM. (A) T2-weighted MR images 7 days after tumor inoculation confirming tumor development. White arrows demarcate tumor boundaries. Tumor volumes between the two treatment groups were not significantly different (unpaired t-test) prior to initiating treatment and equivalence testing suggests 95% confidence that the two groups were equivalent within an interval of ±1 mm^3. Graph shows mean ± standard deviation. **(B)** Continuous temperature monitoring of 9 rats with their device switched on and 4 rats with their device switched off. The remaining 5 normothermia rats did not have temperature monitoring. **(C)** Rat weights through the study period. **(D-E)** Histological sections of brain from a surviving rat after hypothermia treatment. White scale bar = 500 µm. **(D)** Presence of GFP^+ cells (green) below the cooling probe among cells staining for NeuN (red). **(E)** GFP^+ cells (green) did not colocalize with Ki-67 (red) in the surviving rat.

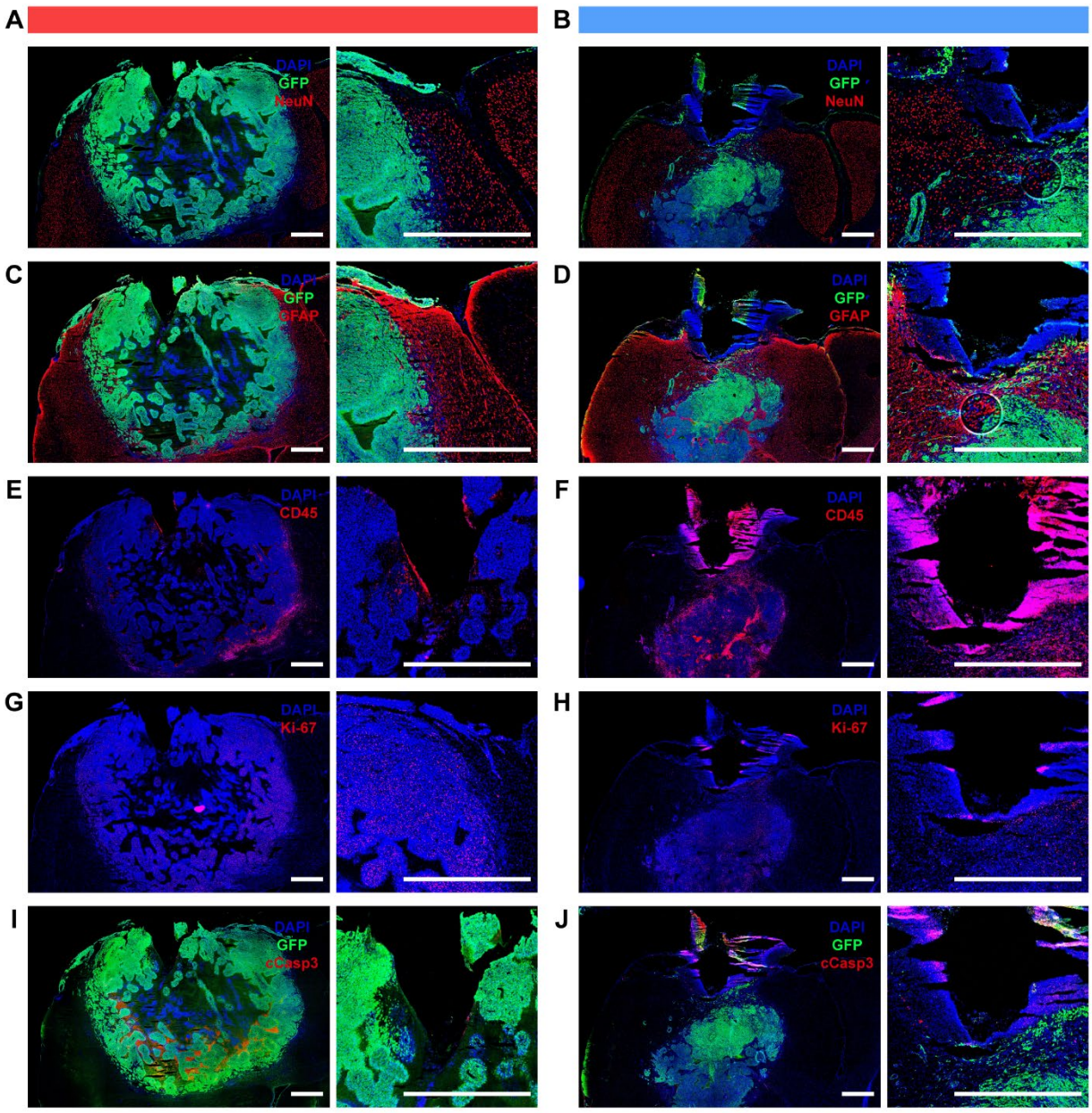

Supplementary Figure 10: Representative immunohistochemistry of Fischer rats with F98 GBM with and without hypothermia. Red bar indicates rat from the normothermia group that was euthanized at ~4 wks after tumor inoculation; blue bar indicates rat from the hypothermia group that was euthanized at ~8 wks after tumor inoculation. **(A-B)** NeuN staining demonstrating intact neuronal nuclei around the tumor (A) and near the hypothermia probe (B). **(C-D)** GFAP staining demonstrating peri-tumoral and ipsilateral reactive gliosis (C) and intact glial populations near the hypothermia probe (D). **(E-F)** CD45 staining to demonstrate leukocyte inflammation within the tumor (E) and within the immediate region adjacent to the hypothermia probe (F). **(G-H)** Ki-67 staining demonstrating proliferative activity in tumor bulk (G) while activity is evidently reduced adjacent to the probe (H). **(I-J)** Cleaved caspase 3 staining demonstrating extensive tumor-intrinsic apoptosis in the rat from the normothermia group (I), and apoptosis in the immediate region around the cooling probe (J). White scale bars = 1000 μm.

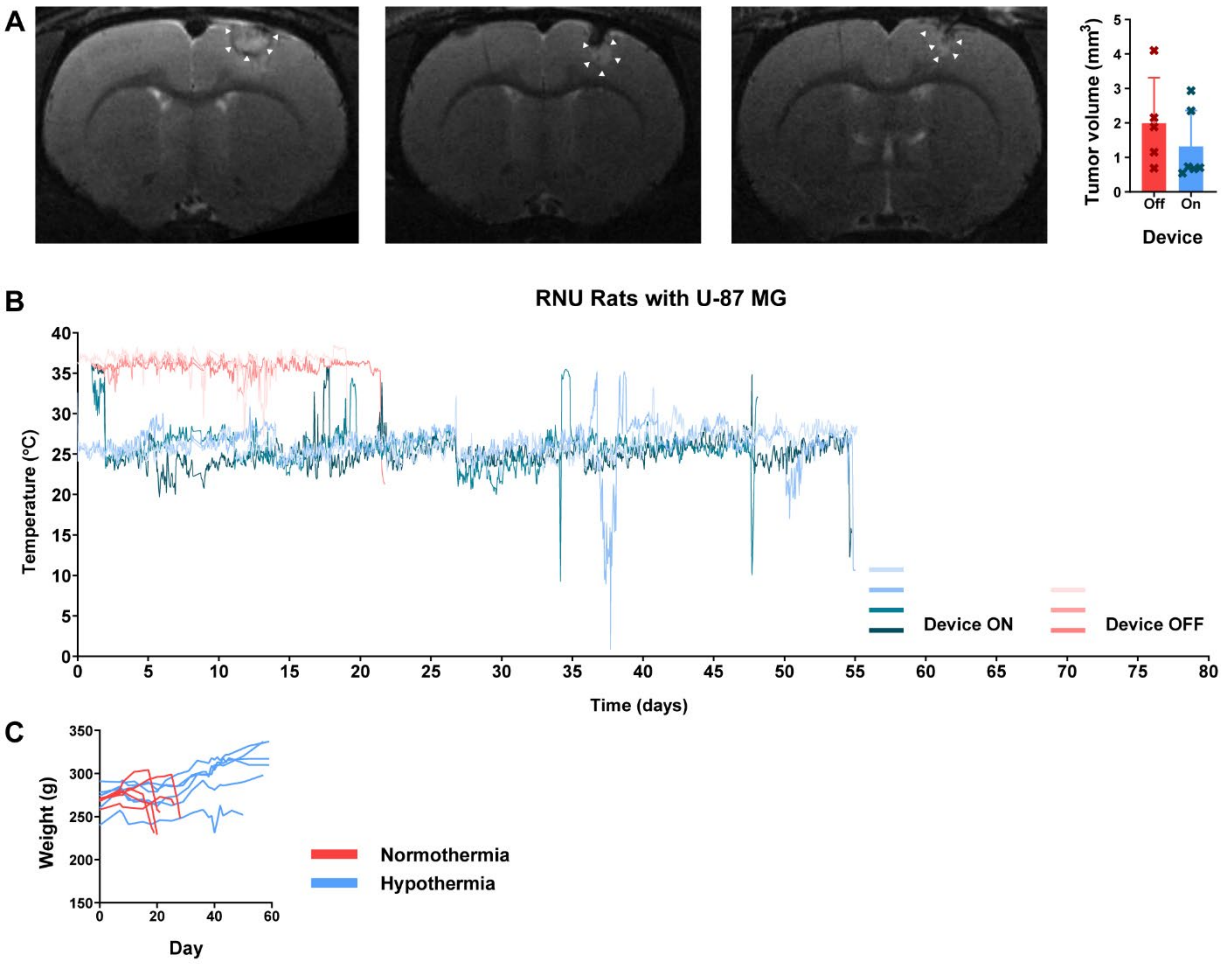

Supplementary Figure 11: Hypothermia treatment of Nude (RNU) rats inoculated with U-87 MG. (A) T2-weighted MR images 7 days after tumor inoculation confirming tumor development. White arrows demarcate tumor boundaries. Tumor volumes between the two treatment groups were not significantly different (unpaired t-test) prior to initiating treatment. Graph shows mean ± standard deviation. **(B)** Continuous temperature monitoring of 4 rats with their device switched on and 3 rats with their device switched off. The remaining 2 treatment rats had premature failure of their thermistors with erratic readings and are thus not displayed. The remaining 2 normothermia rats did not have temperature monitoring. **(C)** Rat weights through the study period.

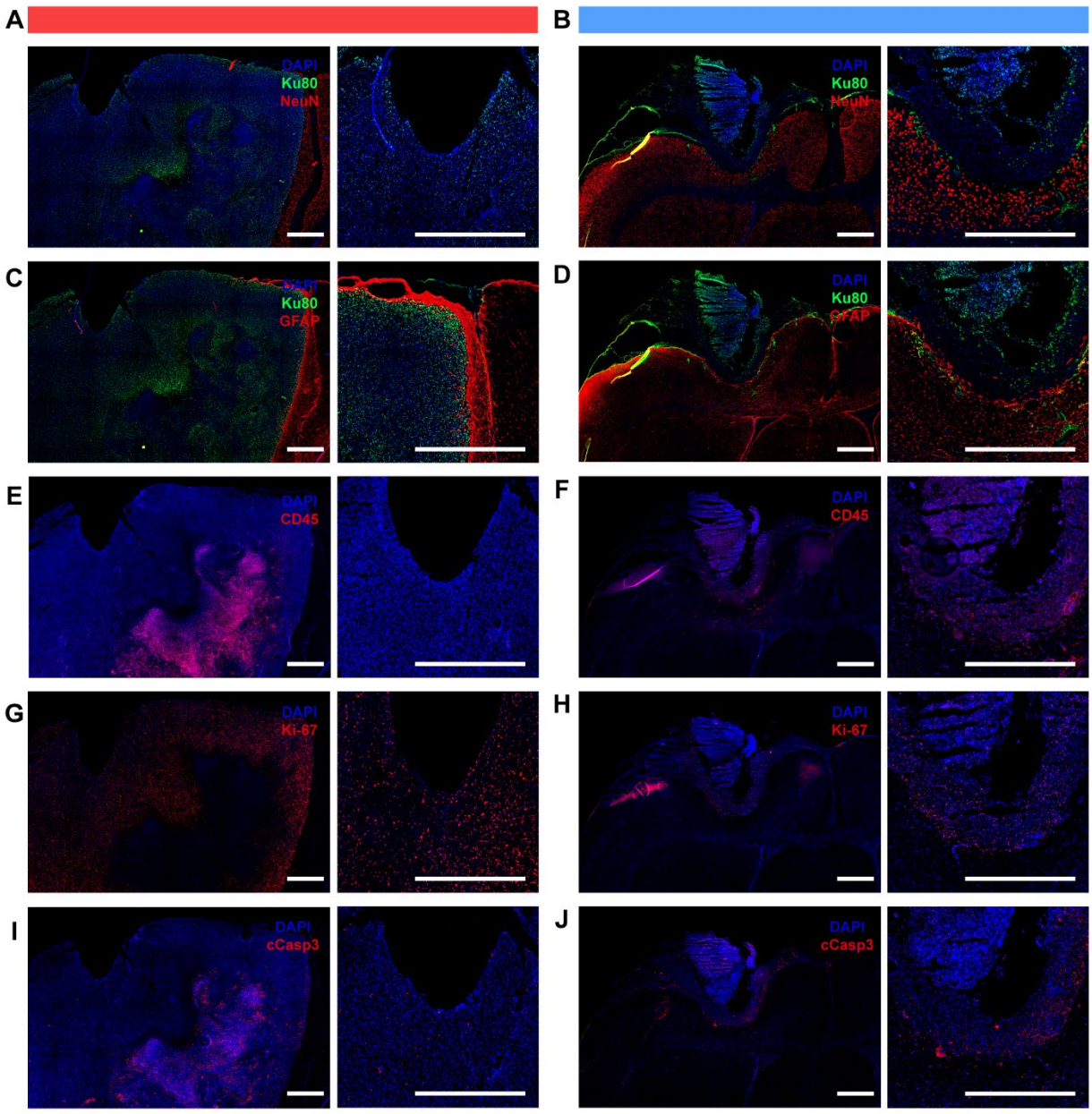

Supplementary Figure 12: Representative immunohistochemistry of RNU rats with U-87 MG with and without hypothermia. Red bar indicates rat from the normothermia group that was euthanized at ~3 wks after tumor inoculation; blue bar indicates rat from the hypothermia group that was euthanized at ~9 wks after tumor inoculation. **(A-B)** NeuN staining demonstrating intact neuronal nuclei around the tumor (A) and near the hypothermia probe (B). **(C-D)** GFAP staining demonstrating peri-tumoral and ipsilateral reactive gliosis (C) and intact glial populations near the hypothermia probe (D). **(E-F)** CD45 staining to demonstrate leukocyte inflammation within the tumor (E) and within the immediate region adjacent to the hypothermia probe (F). **(G-H)** Ki-67 staining demonstrating proliferative activity in tumor bulk (G) and some activity visible adjacent to the cooling probe (H). **(I-J)** Cleaved caspase 3 staining demonstrating extensive tumor-intrinsic apoptosis in the rat from the normothermia group (I), and apoptosis in the immediate region around the cooling probe (J). White scale bars = 1000 µm.

Supplementary Movie 1: RNU and Fischer rats under hypothermia treatment during feeding. Video shows custom cages with either RNU or Fischer rats singly housed being fed while receiving cytostatic hypothermia treatment. Rats can be seen eating bacon softies and grooming themselves.

Supplementary Movie 2: RNU and Fischer rats freely move, groom, and interact under hypothermia treatment. Video shows custom cages with either RNU or Fischer rats singly housed while receiving cytostatic hypothermia treatment. Rats can be seen eating diet gel, freely moving, grooming, and interacting.

Supplementary Table 1: Comparison of well coverage 1 wk after different durations of cytostatic hypothermia (1 to 4 wks) with 1 wk after no hypothermia (0 wks)

Cell line	Temp (°C)	Comparison	adj. *p* -val
U-87 MG	25	0 wks @D07 vs. 1 wk @D14	0.1811
		0 wks @D07 vs. 2 wks @D21	0.0691
		0 wks @D07 vs. 3 wks @D28	**0.0038**
		0 wks @D07 vs. 4 wks @D35	**<0.0001**
T98G	25	0 wks @D07 vs. 1 wk @D14	0.0688
		0 wks @D07 vs. 2 wks @D21	**0.0005**
		0 wks @D07 vs. 3 wks @D28	**<0.0001**
		0 wks @D07 vs. 4 wks @D35	**<0.0001**
LN-229	25	0 wks @D07 vs. 1 wk @D14	**0.0084**
		0 wks @D07 vs. 2 wks @D21	**0.0004**
		0 wks @D07 vs. 3 wks @D28	**0.0024**
		0 wks @D07 vs. 4 wks @D35	**<0.0001**
F98	20	0 wks @D07 vs. 1 wk @D14	**0.034**
		0 wks @D07 vs. 2 wks @D21	0.1849
		0 wks @D07 vs. 3 wks @D28	0.1527
		0 wks @D07 vs. 4 wks @D35	**0.0246**

Two-way ANOVA with Dunnet's multiple comparisons test

Supplementary Table 2: Comparison of cell circularity and size at 25°C and 20°C between Day 0 (37°C) and 3, 7, or 14 days of hypothermia

			Circularity			Average Size		
Cell line	Temp (°C)	Comparison	q	DF	adj. *p* -val	q	DF	adj. *p* -val
U-87 MG	25	D0 vs. D3	2.511	2	0.2378	7.646	2	**0.032**
		D0 vs. D7	29.13	2	**0.0023**	4.154	2	0.1012
		D0 vs. D14	19.2	2	**0.0052**	0.3684	2	0.962
	20	D0 vs. D3	2.291	2	0.2734	5.96	2	0.0517
		D0 vs. D7	3.815	2	0.1179	1.231	2	0.5802
		D0 vs. D14	3.688	2	0.1253	10.64	2	**0.0168**
T98G	25	D0 vs. D3	6.107	2	**0.0494**	6.008	2	0.0509
		D0 vs. D7	2.614	2	0.2234	2.364	2	0.2609
		D0 vs. D14	0.6087	2	0.8741	8.713	2	**0.0248**
	20	D0 vs. D3	0.4372	2	0.9414	5.291	2	0.0647
		D0 vs. D7	2.062	2	0.3183	4.501	2	0.0875
		D0 vs. D14	1.473	2	0.485	0.5521	2	0.8984
LN-229	25	D0 vs. D3	238	2	**<0.0001**	6.934	2	**0.0387**
		D0 vs. D7	13.89	2	**0.0099**	15.62	2	**0.0079**
		D0 vs. D14	45.9	2	**0.0009**	2.982	2	0.1803
	20	D0 vs. D3	22.67	2	**0.0037**	0.4725	2	0.9292
		D0 vs. D7	19.73	2	**0.0049**	0.2619	2	0.9849
		D0 vs. D14	25.11	2	**0.0031**	3.541	2	0.1345
F98	25	D0 vs. D3	9.847	2	**0.0195**	3.786	2	0.1195
		D0 vs. D7	19.96	2	**0.0048**	54	2	**0.0007**
		D0 vs. D14	25.18	2	**0.003**	22.12	2	**0.0039**
	20	D0 vs. D3	2.563	2	0.2304	1.03	2	0.6712
		D0 vs. D7	9.258	2	**0.0221**	1.71	2	0.4078
		D0 vs. D14	10.58	2	**0.017**	1.037	2	0.6678

Two-way ANOVA with Dunnet's multiple comparisons test

Supplementary Table 3: Comparison of F98 circularity and size at Day 0 (37°C), 3, 7, or 14 days between 25°C and 20°C of hypothermia

			adj. *p* -val	
Cell line	Day	Comparison	Circularity	Size
F98	0	25°C vs 20°C	0.9985	0.993
	3	25°C vs 20°C	0.7178	0.9492
	7	25°C vs 20°C	**0.03**	**0.0009**
	14	25°C vs 20°C	**0.0223**	**0.028**

Two-way ANOVA with Šídák's multiple comparisons test

Supplementary Table 4: Comparison of intracellular ATP between Day 3 at 37°C and either Day 3 or Day 7 at 25°C for each cell line

Cell line	Comparison	adj. *p* -val
U-87 MG	Day 3 (37°C) vs. Day 3 (25°C)	0.0999
	Day 3 (37°C) vs. Day 7 (25°C)	**0.0122**
T98G	Day 3 (37°C) vs. Day 3 (25°C)	**0.0057**
	Day 3 (37°C) vs. Day 7 (25°C)	**0.0099**
LN-229	Day 3 (37°C) vs. Day 3 (25°C)	**0.0084**
	Day 3 (37°C) vs. Day 7 (25°C)	**0.0006**
F98	Day 3 (37°C) vs. Day 3 (25°C)	0.1026
	Day 3 (37°C) vs. Day 7 (25°C)	**0.003**

Two-way ANOVA with Dunnet's multiple comparisons test

Supplementary Table 5: Comparison of 24 hour metabolite levels in media after 3 days at different temperatures (20, 25, 30, 37°C) compared to at D0 at 37°C

		Comparison	adj. *p* -val	FDR q
Glucose	U87-MG	37°C D0 vs. 20°C D3	<0.0001	**<0.0001**
		37°C D0 vs. 25°C D3	<0.0001	**<0.0001**
		37°C D0 vs. 30°C D3	0.9453	0.2081
		37°C D0 vs. 37°C D3	<0.0001	**<0.0001**
	T98G	37°C D0 vs. 20°C D3	<0.0001	**<0.0001**
		37°C D0 vs. 25°C D3	0.0033	**0.001**
		37°C D0 vs. 30°C D3	0.002	**0.0006**
		37°C D0 vs. 37°C D3	<0.0001	**<0.0001**
	LN-229	37°C D0 vs. 20°C D4	<0.0001	**<0.0001**
		37°C D0 vs. 25°C D4	0.0154	**0.0043**
		37°C D0 vs. 30°C D4	0.7673	0.1717
		37°C D0 vs. 37°C D4	<0.0001	**<0.0001**
	F98	37°C D0 vs. 20°C D5	<0.0001	**<0.0001**
		37°C D0 vs. 25°C D5	<0.0001	**<0.0001**
		37°C D0 vs. 30°C D5	<0.0001	**<0.0001**
		37°C D0 vs. 37°C D5	<0.0001	**<0.0001**
Lactate	U87-MG	37°C D0 vs. 20°C D6	<0.0001	**<0.0001**
		37°C D0 vs. 25°C D6	<0.0001	**<0.0001**
		37°C D0 vs. 30°C D6	0.7316	0.1664
		37°C D0 vs. 37°C D6	0.5749	0.1365
	T98G	37°C D0 vs. 20°C D7	<0.0001	**<0.0001**
		37°C D0 vs. 25°C D7	<0.0001	**<0.0001**
		37°C D0 vs. 30°C D7	0.6828	0.158
		37°C D0 vs. 37°C D7	0.2967	0.0736
	LN-229	37°C D0 vs. 20°C D8	<0.0001	**<0.0001**
		37°C D0 vs. 25°C D8	<0.0001	**<0.0001**
		37°C D0 vs. 30°C D8	<0.0001	**<0.0001**
		37°C D0 vs. 37°C D8	<0.0001	**<0.0001**
	F98	37°C D0 vs. 20°C D9	<0.0001	**<0.0001**
		37°C D0 vs. 25°C D9	<0.0001	**<0.0001**
		37°C D0 vs. 30°C D9	0.429	0.1046
		37°C D0 vs. 37°C D9	0.5798	0.1365
Glutamate	U87-MG	37°C D0 vs. 20°C D10	<0.0001	**<0.0001**
		37°C D0 vs. 25°C D10	<0.0001	**<0.0001**
		37°C D0 vs. 30°C D10	<0.0001	**<0.0001**
		37°C D0 vs. 37°C D10	<0.0001	**<0.0001**
	T98G	37°C D0 vs. 20°C D11	<0.0001	**<0.0001**
		37°C D0 vs. 25°C D11	<0.0001	**<0.0001**
		37°C D0 vs. 30°C D11	<0.0001	**<0.0001**
		37°C D0 vs. 37°C D11	<0.0001	**<0.0001**
	LN-229	37°C D0 vs. 20°C D12	<0.0001	**<0.0001**
		37°C D0 vs. 25°C D12	<0.0001	**<0.0001**
		37°C D0 vs. 30°C D12	0.0302	**0.0082**
		37°C D0 vs. 37°C D12	<0.0001	**<0.0001**
	F98	37°C D0 vs. 20°C D13	0.0004	**<0.0001**
		37°C D0 vs. 25°C D13	0.1123	**0.0295**
		37°C D0 vs. 30°C D13	0.9678	0.2097
		37°C D0 vs. 37°C D13	<0.0001	**<0.0001**
Glutamine	U87-MG	37°C D0 vs. 20°C D14	<0.0001	**<0.0001**
		37°C D0 vs. 25°C D14	<0.0001	**<0.0001**
		37°C D0 vs. 30°C D14	0.033	**0.0088**
		37°C D0 vs. 37°C D14	<0.0001	**<0.0001**
	T98G	37°C D0 vs. 20°C D15	<0.0001	**<0.0001**
		37°C D0 vs. 25°C D15	<0.0001	**<0.0001**
		37°C D0 vs. 30°C D15	0.2965	0.0736
		37°C D0 vs. 37°C D15	<0.0001	**<0.0001**
	LN-229	37°C D0 vs. 20°C D16	<0.0001	**<0.0001**
		37°C D0 vs. 25°C D16	<0.0001	**<0.0001**
		37°C D0 vs. 30°C D16	0.2893	0.0736
		37°C D0 vs. 37°C D16	0.0086	**0.0024**
	F98	37°C D0 vs. 20°C D17	<0.0001	**<0.0001**
		37°C D0 vs. 25°C D17	<0.0001	**<0.0001**
		37°C D0 vs. 30°C D17	0.9998	0.2132
		37°C D0 vs. 37°C D17	<0.0001	**<0.0001**

ANOVA with Dunnett's multiple comparisons test followed by False Discovery Rate approach for multiple p-values

Supplementary Table 6: Parameters for finite-element modelling of intracranial hypothermia.

Parameter	Value [units]	Source
Brain heat capacity	3630[J/(kg*K)]	Hasgall, P. *et al* . 2018 (30)
Brain density	1046[kg/m^3]	Hasgall, P. *et al.* 2018 (30)
Brain thermal conductivity	0.51[W/(m*K)]	Hasgall, P. et al. 2018 (30)
Brain blood perfusion	0.018, 0.019333, 0.020333 [1/s]	Larkin, J. R. *et al.* 2019 (31)
Tumor multiplier	0.73, 1, 1.52, 3.96	Boxerman, J. L. *et al.* 2006 (32)
Brain/tumor metabolic heat generation	49937[W/m^3]	Wang, Y. *et al.* 2008 (33)
Tumor heat capacity (white brain matter)	3583[J/(kg*K)]	Hasgall, P. et al. 2018 (30)
Tumor density (white brain matter)	1041[kg/m^3]	Hasgall, P. et al. 2018 (30)
Tumor thermal conductivity (white brain matter)	0.48[W/(m*K)]	Hasgall, P. et al. 2018 (30)

Supplementary Table 7: Histological analysis of immediate region adjacent to probe. Brain sections stained with hematoxylin and eosin were analyzed by an expert neuropathologist who was blinded to the groups. After analysis, the data were organized based on treatment groups and labeled "Hypo" for rats that had their devices switched on and "Normo" for rats who had their devices switched off.

Treatment	ID	Periprobe	Areas away from probe not contiguous with periprobe reaction
Hypo	F03	Necrosis with inflammation	no definitive tumor away from probe reaction; deeper tumor shows focal tumor-intrinsic necrosis
Hypo	F05	Necrosis with inflammation	no definitive tumor away from probe reaction; deeper tumor shows extensive tumor-intrinsic necrosis
Hypo	F07	Necrosis with inflammation	no definitive tumor away from probe reaction on sections provided
Hypo	F08	Necrosis with inflammation	Small foci of tumor-intrinsic necrosis; deeper tumor shows extensive tumor-intrinsic necrosis
Hypo	F12	Necrosis with inflammation	no definitive tumor away from probe reaction; deeper tumor shows extensive tumor-intrinsic necrosis
Hypo	F13	Necrosis with inflammation	rim of viable tumor
Normo	F01	probe cavity centered in tumor-intrinsic necrosis	probe cavity centered in large area of tumor-intrinsic necrosis
Normo	F04	Minimal inflammation	large areas of tumor-intrinsic necrosis
Normo	F06	probe cavity centered in tumor-intrinsic necrosis	probe cavity centered in large area of tumor-intrinsic necrosis
Normo	F09	Minimal inflammation	large areas of tumor-intrinsic necrosis
Normo	F10	probe cavity not intact on sections	large areas of tumor-intrinsic necrosis
Hypo	N04	Necrosis with inflammation	no definitive tumor away from probe reaction on sections provided
Hypo	N05	Necrosis with inflammation	no definitive tumor away from probe reaction; deeper tumor shows focal necrosis and large cystic areas
Hypo	N06	Necrosis with inflammation	viable tumor
Hypo	N07	Necrosis with inflammation	no definitive tumor away from probe reaction on sections provided
Hypo	N09	Necrosis with inflammation	viable tumor
Hypo	N10	Necrosis with inflammation	no definitive tumor away from probe reaction on sections provided
Normo	N02	Minimal inflammation; focal mineralized material (?skull)	Small foci of tumor-intrinsic necrosis
Normo	N03	Minimal inflammation	Small foci of tumor-intrinsic necrosis
Normo	N08	Minimal inflammation	large areas of tumor-intrinsic necrosis
Normo	N11	Minimal inflammation	large areas of tumor-intrinsic necrosis
Normo	N12	Minimal inflammation	large areas of tumor-intrinsic necrosis

General observations:

"Small foci of tumor-intrinsic necrosis" show pyknosis (apotosis?) (early ischemic?); associated with at least poly inflammation (can't distinguish apoptosis from mono inflammatory) cells

"Large areas of tumor-intrinsic necrosis" are sometimes geographic/peritheliomatous/cystic, with at least poly inflammation

Periprobe necrosis includes abundant neutrophils around probe cavity, and macrophages more evident further away

"no definitive tumor away from probe reaction on sections provided" means cannot distinguish tumor cells from reactive cells; it does not mean no tumor

The dense DAPI populations around the probe cavity are inflammatory cells; mostly polys, sometimes CD45+ (these may be macrophages or lymphocytes)

Supplementary Table 8: Histological analysis of peritumoral and intratumoral regions. Brain sections stained with either hematoxylin and eosin (H&E) or immunohistochemical markers were analyzed by a Neuropathologist who was blinded to the treatment groups. After analysis, the data are labeled "Hypo" for rats that had their devices switched on and "Normo" for rats who had their devices switched off.

		Peritumoral findings on H&E				Intratumoral findings on H&E			Peritumoral (PT) and neuropil (NP) immunofluorescent staining				
Treatment	**ID**	**edema**	**hemorrhage**	**hypercellularity**	**vascular changes**	**necrosis**	**VRSi**	**tumor size**	**GFAP gliosis**	**Ki67**	**NeuN**	**CD45**	**CC3**
Hypo	F03	moderate	_	moderate	moderate	yes	yes	medium	diffuse to edge of cortex	CTT	intact	mod PT, minimal NP	minimal NP
Hypo	F05	moderate	_	mild	moderate	yes	yes	medium	extensive around tumor	CTT	intact	mild PT, minimal NP	_
Hypo	F07	moderate	_	moderate	moderate	yes	_	small	extensive around tumor	scatter @ border	intact	mild PT	mild NP
Hypo	F08	moderate	_	mild	moderate	_	yes	large	extensive around tumor	few @ border	intact	mild PT	stain failed
Hypo	F12	marked	_	moderate	moderate	yes	yes	medium	peritumoral	few @ border	intact	mod PT, minimal NP	mild NP
Hypo	F13	moderate	_	moderate	moderate	yes	_	small	peritumoral	scatter @ border	intact	mod PT, minimal NP	mild NP, and PT
Normo	F01	moderate	_	mild	_	yes	yes	large	diffuse to edge of cortex	CTT	intact	dense PT, minimal NP	minimal NP
Normo	F04	moderate	_	mild	_	yes	_	large	extensive around tumor	CTT	intact	dense PT, minimal NP	_
Normo	F06	moderate	_	moderate	_	yes	yes	medium	diffuse to edge of cortex	CTT	intact	mod PT, mild NP	_
Normo	F09	moderate	mild fresh	marked	_	yes	yes	medium	extensive around tumor	few @ border	intact	mod PT, minimal NP	mild NP
Normo	F10	moderate	_	moderate	mild	yes	yes	medium	stain failed	stain failed	stain failed	stain failed	stain failed
Hypo	N04	mild	_	moderate	mild	yes	_	small	peritumoral	scatter @ border	intact	stain failed	mild NP, and PT
Hypo	N05	moderate	_	mild	mild	yes	_	small	extensive around tumor	scatter @ border	intact	stain failed	_
Hypo	N06	mild	mild fresh	mild	_	yes	_	small	peritumoral	CTT	intact	stain failed	minimal NP
Hypo	N07	_	mild fresh	_	mild	yes	_	small	diffuse to edge of cortex	scatter @ border	intact	stain failed	minimal NP
Hypo	N09	mild	focal old	mild	moderate	yes	_	medium	peritumoral	CTT	intact	stain failed	minimal NP
Hypo	N10	mild	_	mild	mild	yes	_	small	peritumoral	CTT	intact	mild PT	minimal NP
Normo	N02	mild	_	mild	mild	_	_	large	peritumoral	stain failed	intact	stain failed	_
Normo	N03	_	_	_	_	_	_	large	peritumoral	CTT	intact	minimal PT	minimal NP
Normo	N08	_	_	_	_	yes	_	large	diffuse to edge of cortex	CTT	intact	stain failed	minimal NP
Normo	N11	mild	_	mild	_	yes	_	large	peritumoral	CTT	intact	minimal PT	minimal NP
Normo	N12	_	_	_	_	yes	_	large	peritumoral	stain failed	intact	stain failed	minimal NP

General observations:

No evidence of peritumoral or distant infarction or vascular thrombosis in any brain
No evidence of infection (no neutrophilic encephalitis or meningitis, no bacterial or fungal colonies evident on H&E) in any brain
No evidence of herniation (no effacement of CSF spaces) in any brain
No loss of NeuN staining; intact to border of tumor on all sections
No evidence of diffuse infiltration of glioma
Vascular changes: microvessel dilation and/or hyperplasia
All reactions are ipsilateal to tumor, including reactive gliosis; no contralateral effect other than mass effect
Ki67 is largely confined to tumor (CTT) except where otherwise noted
VRSi = Virchow-Robin space involvement
CD45 will stain macrophages, lymphocytes and microglia
From one area to another, features can change a level, from none to mild to moderate to marked, so sampling error must be considered